2015 IEEE International Conference on Computer and Information Technology; Ubiquitous Computing and Communications; Dependable, Autonomic and Secure Computing; Pervasive Intelligence and Computing

Method to Develop Coded Excitation for Velocimetry in Downhole Drilling

Weijia Lu, Ran Niu, Longtao Yuan, Xin Qu, Heng Wu, Jing Ye
GE Global Research, Shanghai, China

***Abstract*—Background: In this paper, the phase modulation coding/decoding technology is discussed for the application in the high attenuation medium based on the simulation and the experiment. Methods: For the decoding perspective, the matched filter and the inverse filter are compared. An extra processing is introduced right after the matched filtering to restrain the range sidelobes. Furthermore, in the latter part of this paper, the factors to cause a degeneration in signal-noise ratio are quantitatively evaluated by simulation beam pattern and Doppler signal. Results: Based on the experiments and simulation in this paper, it's found that the signal amplitude get significant boosted (30dB) while the range resolution is compatible with the span of a single pulse. It's also proved that the frequency dependent phase distortion from attenuation will cause more degeneration than Doppler effect, but even this influence can be compensated by the equalization.**

***Keywords*-Pulse Compression, Attenuation Model, Simulation, Decoding.**

I. Introduction

In the past decades, Doppler flow detection has been used in the downhole drilling [1]–[3]. In a conventional pulse wave ultrasound, several pulses are launched into the medium, the scattering signals received are range gated, from which the Doppler frequency shifts are extracted to depict the velocity profile [1]. The transmitted waveform is long enough to overwhelm the attenuation from medium [4], and provides a good frequency resolution for the Doppler shift analysis. However, a longer pulse, or an equivalent smaller bandwidth in frequency, results in a poor axial/range resolution, which could make the adjacent targets indistinguishable or lead to a bad prediction on the flow velocity profile [1], [5]–[8]. To conquer this sensitivity/resolution trade-off, in the medical ultrasound, a coded excitation is used [9]–[12]. A most seductive reason to reuse this technology in the drilling business, relies on the lacking of those limitation coming from the biosafety consideration in a healthcare application (ISPTA, MI, etc [13]).

A conventional coded excitation ultrasound could be described as the following signal chain [10]: (a) an elongated excitation waveform generation module, with *a priori* code strategy, to pursue an enough penetration in the propagation path; (b) the conventional pulse-wave system, e.g. including transducer, time gain compensation (TGC), in-phase and quadrature (I/Q) demodulation and decimation, equalization and post-processing based on different modules; (c) the decoding module designed following the same code strategy, to further boost the signal-to-noise ratio (SNR) and the range resolution. The part (a) is usually performed by the hardware circuit, constrained by its capability. And part (c), either implemented by the hardware or the software, usually costs extra efforts in designing. And in the most case the method to implement this part can be divided into two categories: a matched filter or an inverse filter. Moreover, this part can be either put before the I/Q demodulation, or after.

For the code strategy, there are always dozens of options: the amplitude modulation is always out of the scope in ultrasonic application, since not all energy is transformed into the mechanical wave; the frequency modulation codes, e.g linear FM (aka chirp), tapered linear FM or a non-linear one, are widely used, but these code strategies need extra design in hardware [14], [15]; in the phase modulation family, or the binary code denoting two-phase modulation, barker codes and golay codes are very famous, but golay codes, usually in a pair, suffer the mismatch from the motions of the target [11].

In a binary code system, the basic excitation waveform is modulated by a specific length of binary sequence (aka. chips [11]), thus the basic excitation waveform is also called as chip wave. Normally, the formation of the chip wave is restrained by the levels of voltage provided by the circuit. But an optimized solution can always be pursued, e.g. the multiple-level chip wave could have better transform efficiency than the square wave, with the major benefit coming from the spectrum wise similarity to the transducer.

In this paper, we concern ourselves with the migration of the coded excitation into the downhole drilling application. The discussion starts from the discrete formulation of the coding/decoding processing. For the code strategy, considering a simplified design of the excitation circuit, as well as the motions of the targets, barker codes modulated square chip wave are used. In the decoding, two implementation methods are both investigated, and the processing is on the radio-frequency (RF) signal before demodulation. In the later part of this paper, the experiment is involved to test the theorem formulated method. And the simulation is conducted to quantify the degeneration factors from the specific drilling scenario.

II. Methodology

A. Firing with the coded pulse and decoding with a matched filter

We consider the excitation wave $W(n)$ transmits through the probe, whose impulse response equal to $PB(n)$. $W(n)$ is a wave sequence built from the basic chip wave $CP(n)$. Each chip wave has length equal to T_n. $CD(n)$ is several bits of modulation code. For instance it is [+1, +1, +1, -1, +1] for **5**bits

978-1-5090-0154-5/15 $31.00 © 2015 IEEE
DOI 10.1109/CIT/IUCC/DASC/PICOM.2015.127

barker code. Thus a discrete form can be written to denote transmitted pulse $Tx(n)$ into the medium through the probe.

$$\begin{aligned} Tx(n) &= W(n) \underset{n}{\otimes} PB(n) \\ &= \sum_k CD(k)\delta(n-kT_n) \underset{n}{\otimes} CP(n) \underset{n}{\otimes} PB(n) \end{aligned} \tag{1}$$

During the decode phase (traditionally can also be called compression), a matched filter $W(-n)$ is firstly introduced, thus we can represent the received signal $Rt(n)$ as following expression,

$$\begin{aligned} Rt(n) &= Tx(n) \underset{n}{\otimes} Att(n) \underset{n}{\otimes} Scat(n) \underset{n}{\otimes} Att(n) \underset{n}{\otimes} PB(n) \underset{n}{\otimes} W(-n) \\ &= Rt^{'}(n) \underset{n}{\otimes} W(-n) \\ W(-n) &= \sum_k CD(k)\delta(-n+kT_n) \underset{n}{\otimes} CP(-n) \end{aligned} \tag{2}$$

Then a constant value simply substitute for the medium attenuation $Att(n)$ and scattering $Scat(n)$, before bringing them back into the discussion later. Moreover, we switch the calculation order, associate the corresponding terms, and define $\mu(n)$ as the oversampling of the auto-correlation ($AR_{\square}(n)$) of the code bits $CD(n)$, thus

$$\begin{aligned} \mu(n) &\triangleq \sum_k CD(k)\delta(n-kT_n) \underset{n}{\otimes} \sum_k CD(k)\delta(-n+kT_n) \\ &= \sum_k AR_{CD}(k)\delta(n-((k+1)T_n-1)) \\ Rt(n) &= \mu(n) \underset{n}{\otimes} AR_{CP}(n) \underset{n}{\otimes} PB^{'}(n) \end{aligned} \tag{3}$$

$PB^{'}(n)$ in (3) is a convolution of the probe's impulse response by itself. If one consider the symmetric of a Gaussian wave, as is usually used to describe an ideal probe. This term can also be approximated by the auto-correlation as well.

B. An extra effort to restrain range sidelobes

It is well known that the auto-correlation brings a constant ripples, which causes the axial/range sidelobes to decrease the resolution. Thus, a FIR filter is introduced on the matched filter's output to suppress this artifact [16]. As the barker code is used, constant ripples in $AR_{CD}(n)|_{n=1\ldots2M-1}$ will has a magnitude equal to $1/M$ (M is the sum of code bits). If the FIR filter $b_{1\ldots n}$ is well designed to remove all ripples on $AR_{CD}(n)$, there is nothing left but the mainlobe. Moreover, it is also convenient for this FIR filter to has a limited number of odd symmetric coefficients ($= 2N-1$, $N < M$). With this two assumptions, we can write down the convolution as following matrix operation,

$$\begin{bmatrix} AR_M & \cdots & AR_{M-N+1} \\ \vdots & \ddots & \vdots \\ \cdots & \cdots & AR_{M-N+M} \end{bmatrix} \begin{bmatrix} b_N \\ \vdots \\ b_{2N-1} \end{bmatrix} = [AR^{'}][b^{'}] = \begin{bmatrix} m \\ \vdots \\ 0 \end{bmatrix} = [Y] \tag{4}$$

In (4), $[AR^{'}]$ and $[b^{'}]$ are both the part of the corresponding matrix since the symmetry, and because of the same reason, in the right hand of (4), the mainlobe is the first sample of the output signal. Based on the (4), FIR taps is equal to the pseudo inverse of $[AR^{'}]$ multiplied by $[Y]$.

With the help of this filter on the time/range axis, most of the ripple could be restrained while the signal in the mainlobe is mostly reserved. To further use this filter into a system described as (3), the similar oversampling operation should be conducted.

C. Frequency sampling to design an inverse filter for the decoding

Instead of a matched filtering in (2), an oversampled inverse filter $SP(n)$ could be used (also called spiking filter),

$$\begin{aligned} Rt(n) &= Tx(n) \underset{n}{\otimes} Att(n) \underset{n}{\otimes} Scat(n) \underset{n}{\otimes} Att(n) \underset{n}{\otimes} PB(n) \underset{n}{\otimes} SP(n) \\ SP(n) &= \sum_k Sp(k)\delta(n-kT_n) \underset{n}{\otimes} CP(-n) \\ \nu(n) &\triangleq \sum_k CD(k)\delta(n-kT_n) \underset{n}{\otimes} \sum_k Sp(k)\delta(n-kT_n) \\ &= \sum_k (CD(k) \underset{k}{\otimes} Sp(k))\delta(n-((k+1)T_n-1)) \\ Rt(n) &= \nu(n) \underset{n}{\otimes} AR_{CP}(n) \underset{n}{\otimes} PB^{'}(n) \end{aligned} \tag{5}$$

The spiking filter's coefficients Sp is designed based on the code chips, to inverse the spectrum of code in a sense of least squares optimization [7], [8]. During the estimation of the filter's coefficients, L frequency bins evenly distributed over unit cycle is firstly chosen on FFT spectrum,

$$\begin{aligned} S(f_k) &= \sum_{i=0}^{M-1} CD(i)e^{-j2\pi\frac{ik}{L}}|_{k=1\ldots L} \\ [S]_{L\times1} &= [W]_{L\times M}[CD]_{M\times1}, \text{where } W_{ki} = e^{-j2\pi\frac{ik}{L}} \end{aligned} \tag{6}$$

To find an inverse system $[D] = \widehat{[S]^{-1}}$, the expected spiking filter Sp could be approximated by $\widehat{Sp}$,

$$\widehat{Sp} = (W^*W)^{-1}W^*D \tag{7}$$

III. Experiment and Discussion

A. Comparing result in experiment

To further verify the theorem formulated method, a wire target is merged into the water tank, illuminated by an ultrasonic probe for test (60%BW_f, 500KHz). The probe is fired by the sequence modulated by **5**bits barker code, with a square wave (1-cycle, 50% duty cycle) as its basic chip waveform. The backscattering signal is decoded by (a) a matched filter plus a **9**taps sidelobe restrain filter, and (b) **32**taps inverse filter. The results are compared in Fig.1.

The figure shows if we use a detection system with a constant dynamic range (=15dB), the original receive signal without the pulse compression, will have two peaks linking to the same single physic target (n = $500-600$, $620-670$). On the other hand, the pulse compression by **5**bits barker code narrows the main peak, meanwhile amplifies the signal. It is also shown that the inverse filter (red line) provides smaller range sidelobe comparing with the output from the matched filer (blue line).

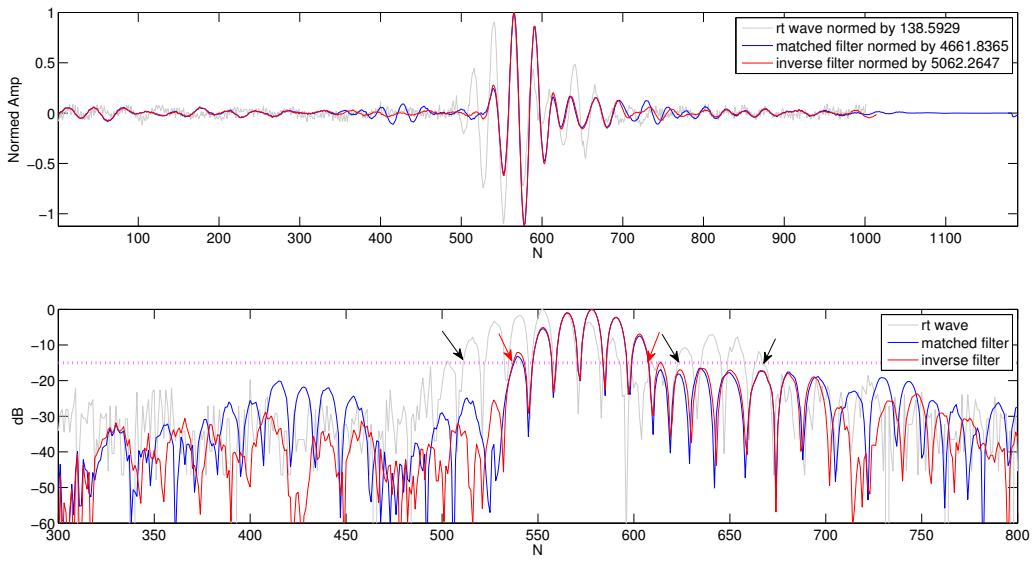

Fig. 1. Compare the compressed RF signals using different decode methods in experiment. The span of the range peak after inverse filter/matched filtering are marked by the red arrow pairs, and the span in the uncompressed wave are marked by the black arrow pairs. The dynamic range of the detection system = -15dB, which is less than the range sidelobe level in a **5**bits barker code system ($20\log_{10}(1/5)$ = -14dB)

B. Factors to degenerate the SNR in the pulse compression system

In the ultrasound system, the inherent SNR can be defined on the instantaneous maximum intensity ($I_{peak} = P_{max}^2/\rho c$) [9]. The theoretical boost in the SNR by the pulse compression is $10\log_{10}$M (M is the sum of code bits), if the barker code family is used [11]. In a real dispersive medium, two major concerns should be raised, all of which cause a degeneration on the SNR: (a) the frequency dependent phase distortion from attenuation [17]; (b) the influence from Doppler effects [12]. In the paper of Rao et als's, the speckle is also included as a factor. But here only additive noise is considered in the SNR analysis.

TABLE I. Acoustic characteristic in mud

Density of Mud in lb/gal	α_0	β	Attenuation† in dB/inch	c
9	5.36	0.87	4.5	1185
11	7.75	..	6.5	..
13	10.73	..	9	..
15	11.92	..	10	..
17	11.32	..	9.5	..
19	9.54	..	8	..

† In this column, we use attenuation value [dB/inch @ 280KHz] in OBFs reported by [18]. The α_0 [dB/(cm·MHz)] is then estimated from these value after a reasonable setup of β = 0.87 (based on the measurement read)

C. The attenuation of the drilling fluid and equalization

To examine the degeneration level, the attenuation of the oil based fluid (OBF) should firstly be measured since its relative bigger influence [18]. Later on an frequency dependent attenuation model could be regressed from these measurements, which follows the power law, and could be written down as following,

$$\alpha(f) = \alpha_0 \times f^{\beta}, \text{where } \beta \text{and } \alpha_0 \text{ as in table I} \qquad (8)$$

With the attenuation model, the test pulse waveform for examination is generated through the MATLAB simulation by solving KZK equation under different attenuation situation [19]. In the following simulation study, instead of using the measured value, we use the deducted one (in table I) based on the Motz's report [18]. Before the simulation, the ultrasonic system is configured following a common setup in the downhole drilling (central frequency f_0= 500KHz, fractional bandwidth = 0.6, the aperture size = 50mm in azimuth and elevation direction). During the simulation, the same excitation wave sequence is used as the one for experiment. The beam profile (Fig.2a), and the spectrum of the on-axis waveform in corresponding depth, normalized to its mainlobe (Fig.2b) are calculated to evaluate the attenuation influence. The on-axis waveforms are further saved, to test two aforementioned decode methods. The degeneration of SNR is late denoted by the change on the decibel maximal magnitudes of the compressed waveforms, in the different attenuation scenario (Fig.2c).

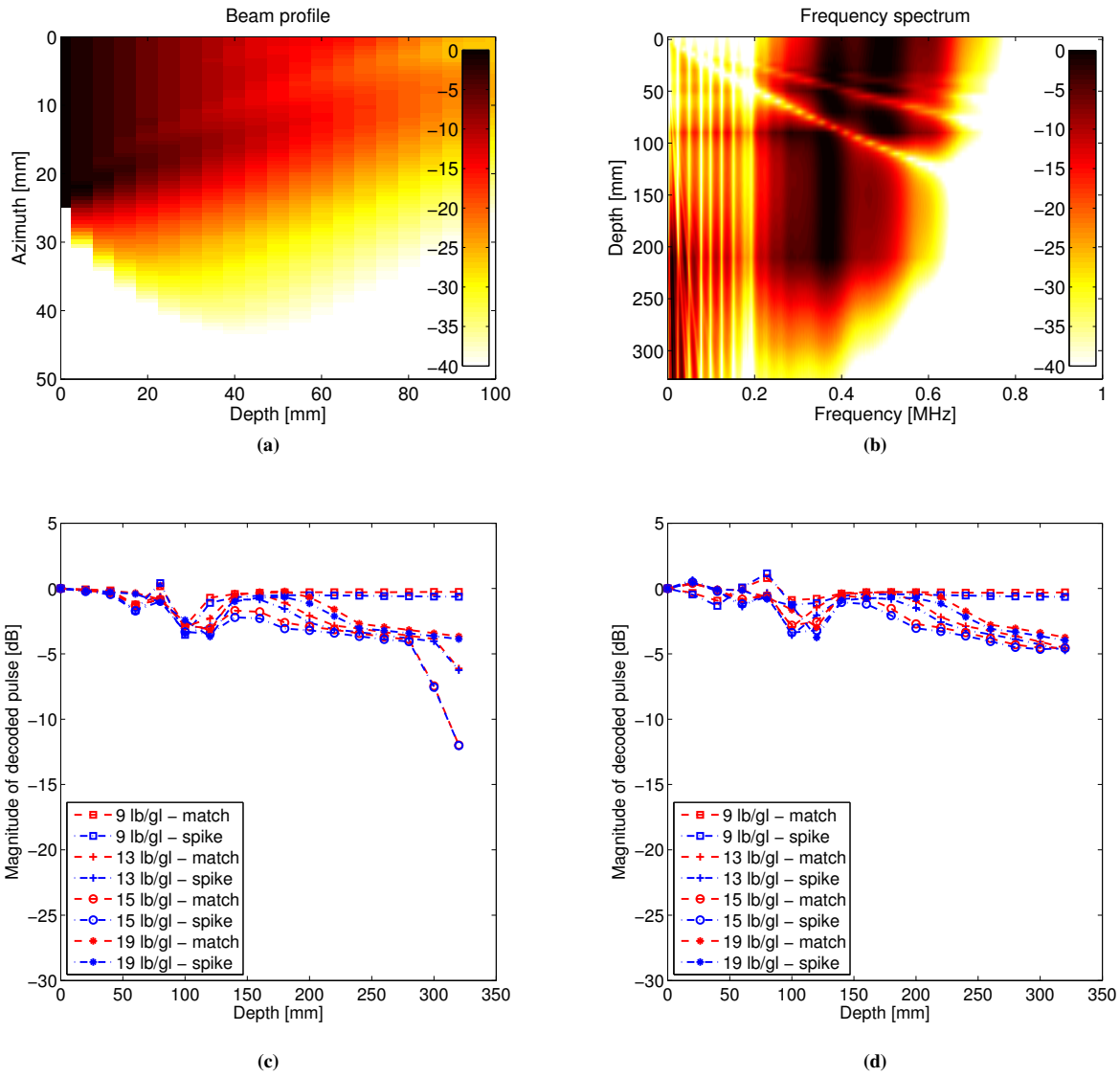

Fig. 2. (a) The beam profile on the cross-section in 15lb/gl OBF, (b) The frequency related distortion from the attenuation in 15lb/gl OBF, (c) Compare the magnitude of the compressed waveform in different OBF without compensation from equalization, (d) Compare the magnitude of the compressed waveform while equalization is involved.

During the generating of Fig.2c, the test on-axis pulse is firstly normalized to unit, thus the degeneration shown on the figure is only from the frequency distortion brought by the attenuation. From the Fig.2c, it is observed that in the **300**mm away from the aperture, the decoded waveforms in **15**lb/gal OBF have more than **-5**dB degeneration. To compensate the degeneration from the attenuation, the equalization can be introduced. In our case, the *a priori* knowledge about the attenuation could help restoring the uncontaminated pulse spectrum, once the corresponding detection range is known. Fig.2d gives the decibel magnitude of the decoded waveform after the equalization, and none of them suffer more than **-5**dB degeneration.

D. The degeneration from Doppler effect

The type of the particle, scattering most of the acoustic wave in the drilling fluid, is drilled solids (sands, gravels , cuttings etc.). Other components like barite ($\phi < 74$um) and bentonite ($\phi < 2$um) (ref to [20]) are too small to cause a diffractive scattering (since wavenumber-diameter product $k\phi \ll 1$) [21], even their relatively big mismatch in impedance. Thus the Doppler signals detected reflect the movement of drilled solids, which usually has a total volume concentration less than 10% [20]. Because of such a small concentration,

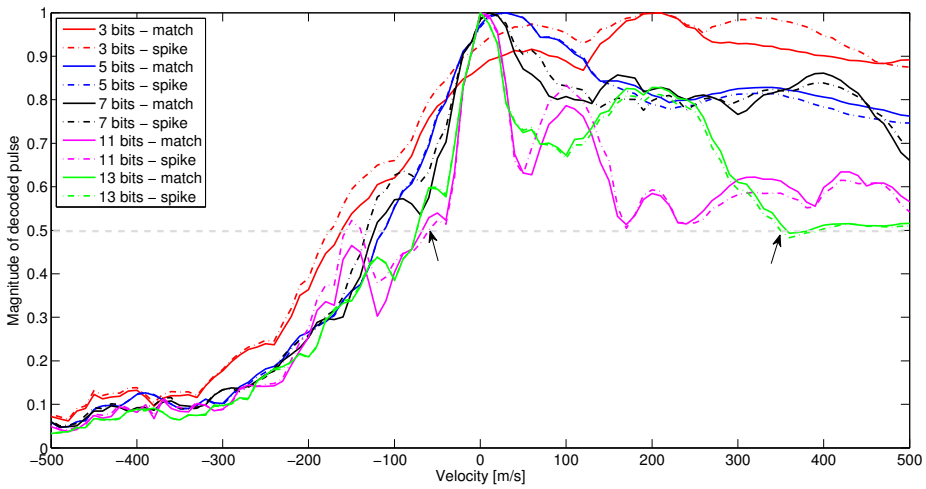

Fig. 3. The magnitude degeneration from Doppler effect under diverse code. The chipwave used is 50% duty cycle square wave, central frequency is 500KHz, and the fractional bandwidth is 60%.

the Doppler signal in a range volume can be interpreted as the superposition of the scattering from each particle, rather than represented as the fluctuations of a continuum medium [22]. For the scattering of a single moving particle, it is a dilated replica of the transmitted pulse, with the resampling ratio a controlled by the on-axis velocity v_a through the following well-known equation [23],

$$a = 1 + \frac{2v_a}{c} \tag{9}$$

Lately, the aforementioned decode method is tested on these test pulse, and result is shown in Fig.3. It can be read that a $-6dB$ cut off happens once the particle is moving in a speed of 50m/s away from the aperture, or 350m/s toward to the aperture. Since these two velocities are far away from the common velocity of the mud, the degeneration from Doppler effect can be ignored comparing with the counterpart from the attenuation.

E. Range resolution in both method

The range resolution of the compressed pulse is mostly governed by the probe and the chipwave, i.e. $AR_{CP}(n) \underset{n}{\otimes} PB^{'}(n)$ in (3) and (5), after the sidelobes of $\mu(n)$ in (3) is suppressed or a carefully designed spiking filter removes the modulation from the code. Same statement can be found in the Kristoffersen's paper [24].

IV. Conclusion

To resolve the sensitivity/resolution trade-off in Doppler flow detection, the phase modulation coded (barker code) excitation is reused in the downhole drilling application, two compression (decode) strategies have been properly formulated and experimental verified. In the experiment, both methods show an amplification on the signal ($\approx 30dB$ in Fig.1) while the span of range mainlobe is close to a single chip length ($N \approx 60$ whilst it is 50 in a single chip in Fig.1). Moreover, one can find inverse filter has smaller range sidelobe than the matched filter. But the spiking filter has much longer taps (the spiking filter has 32 taps whilst matched filter has only 5 taps pulsing a 9 taps of FIR filter to suppress sidelobe).

Later on, the degeneration of SNR, caused by Doppler effect and the attenuation, are investigated by simulation. In the simulation, the estimated attenuation model is involved based on previous report. From these analysis, we can claim that the influence from Doppler effort can be ignored in this application, while the frequency distortion from the mud's attenuation can be compensated by a proper designed equalization operation.

References

[1] A. Shekarriz and D. M. Sheen, "Method and apparatus for ultrasonic doppler velocimetry using speed of sound and reflection mode pulsed wideband doppler," May 30 2000, uS Patent 6,067,861.

[2] S. Huang, "Doppler flowmeter for multiphase flows," Jul. 6 2004, uS Patent 6,758,100.

[3] W. Han, J. M. Beique, J. R. Birchak, A. T. Hemphill, T. Wiemers, and P. F. Rodney, "Acoustic doppler downhole fluid flow measurement," Sep. 6 2005, uS Patent 6,938,458.

[4] H. Azhari, *Basics of biomedical ultrasound for engineers*. John Wiley & Sons, 2010.

[5] S. G. Foster, P. M. Embree, and W. D. O'Brien, "Flow velocity profile via time-domain correlation: Error analysis and computer simulation," *Ultrasonics, Ferroelectrics and Frequency Control, IEEE Transactions on*, vol. 37, no. 3, pp. 164–175, 1990.

[6] T. Misaridis and J. A. Jensen, "Use of modulated excitation signals in medical ultrasound. part i: Basic concepts and expected benefits," *Ultrasonics, Ferroelectrics and Frequency Control, IEEE Transactions on*, vol. 52, no. 2, pp. 177–191, 2005.

[7] F. Gran and J. A. Jensen, "Designing waveforms for temporal encoding using a frequency sampling method," *IEEE Trans Ultrason Ferroelectr Freq Control*, vol. 54, no. 10, pp. 2070–2081, Oct 2007.
[8] F. Gran, J. Udesen, M. B. Nielsen, and J. A. Jensen, "Coded ultrasound for blood flow estimation using subband processing," *IEEE Trans Ultrason Ferroelectr Freq Control*, vol. 55, no. 10, pp. 2211–2220, Oct 2008.
[9] M. O'Donnell, "Coded excitation system for improving the penetration of real-time phased-array imaging systems," *IEEE Trans Ultrason Ferroelectr Freq Control*, vol. 39, no. 3, pp. 341–351, 1992.
[10] B. Haider, P. A. Lewin, and K. E. Thomenius, "Pulse elongation and deconvolution filtering for medical ultrasonic imaging," *IEEE Trans Ultrason Ferroelectr Freq Control*, vol. 45, no. 1, pp. 98–113, 1998.
[11] R. Y. Chiao and X. Hao, "Coded excitation for diagnostic ultrasound: a system developer's perspective," *IEEE Trans Ultrason Ferroelectr Freq Control*, vol. 52, no. 2, pp. 160–170, Feb 2005.
[12] H. Zhao, L. Y. Mo, and S. Gao, "Barker-coded ultrasound color flow imaging: theoretical and practical design considerations," *IEEE Trans Ultrason Ferroelectr Freq Control*, vol. 54, no. 2, pp. 319–331, Feb 2007.
[13] B. Lamboul, M. Bennett, T. Anderson, and N. Mcdicken, "Basic considerations in the use of coded excitation for color flow imaging applications," *Ultrasonics, Ferroelectrics, and Frequency Control, IEEE Transactions on*, vol. 56, no. 4, pp. 727–737, 2009.
[14] O. Lowenschuss and R. Roy, "Pulse compression radar," Dec. 3 1974, uS Patent 3,852,746.
[15] C. Miller, "Fm pulse compression radar," Sep. 6 1977, uS Patent 4,047,173.
[16] B. R. Mahafza, *Radar Systems Analysis and Design Using MATLAB*. CRC Press, LLC, 2013.
[17] N. A. Rao, "Investigation of a pulse compression technique for medical ultrasound: a simulation study," *Med Biol Eng Comput*, vol. 32, no. 2, pp. 181–188, Mar 1994.
[18] E. Motz, D. Canny, E. Evans *et al.*, "Ultrasonic velocity and attenuation measurements in high density drilling muds," in *SPWLA 39th Annual Logging Symposium*. Society of Petrophysicists and Well-Log Analysts, 1998, pp. 1282–1285.
[19] M. Frijlink, H. Kaupang, T. Varslot, and S. Masoy, "Abersim a simulation program for 3d nonlinear acoustic wave propagation for arbitrary pulses and arbitrary bibliography," in *Proceedings of Ultrasonics Symposium, 2008. IUS 2008. IEEE*, Nov. 2008.
[20] A. S. S. Committee *et al.*, *Drilling fluids processing handbook*. Elsevier, 2011.
[21] T. L. Szabo, *Diagnostic ultrasound imaging: inside out*. Academic Press, 2004.
[22] B. A. Angelsen, "A theoretical study of the scattering of ultrasound from blood," *Biomedical Engineering, IEEE Transactions on*, no. 2, pp. 61–67, 1980.
[23] A. Hajjam and H. Behnam, "A modified time-domain approach for modelling the ultrasound signal from blood-flow," *Ultrasound*, vol. 16, no. 3, pp. 160–164, 2008.
[24] K. Kristoffersen, "Optimal receiver filtering in pulsed doppler ultrasound blood velocity measurements," *Ultrasonics, Ferroelectrics, and Frequency Control, IEEE Transactions on*, vol. 33, no. 1, pp. 51–58, 1986.